Instances of Mixed Buckling and Post-Buckling of Steel RHS Beams

Noureddine Ziane[1]*, Giuseppe Ruta[2], Sid Ahmed Meftah[1], Moustafa Hadj Doula[1], Noureddine Benmohammed[1]

[1] Laboratoire des Structures et Matériaux Avancés dans le Génie Civil et Travaux Publics, Université de Djillali Liabes, Sidi Bel Abbes, Algeria.
[2] Department of Structural & Geotechnical Engineering, University 'La Sapienza', and National Group for Mathematical Physics, Rome, Italy.

Abstract
Simply supported steel beams with rectangular hollow section (RHS) are investigated, taking into account large twist and cross-sections distortions. A closed-form expression for the critical value of the external couple inducing lateral torsional buckling is found; homotopy perturbation method (HPM) is used to investigate the post-buckling non-linear path. The linear and non-linear paths given by HPM are compared to those of: i) a Newton–Raphson algorithm with arc length; and ii) the commercial FEM code Abaqus. Some numerical examples are presented.

Keywords: RHS steel beams; Distortion; Post-buckling; Homotopy; Newton–Raphson

1. Introduction

Thin-walled beams with RHS have high strength- and stiffness-to-weight ratios, thus they are largely used. Thin-walled beams (TWB) were comprehensively modelled first by Vlasov [1], while Benscoter [2] investigated TWB with closed cross-sections.

Box beams with rigid cross-sections in a linear setting were considered, among others, by Smith and Chopra [3], Shakourzadeh et al. [4], Kim and White [5], Loughlan and Ata [6], Pluzsik and Kollar [7], Ziane et al. [8]. Later on, the cross-section was no more supposed to be rigid: Mentrasti [9] studied RHS undergoing shear in their walls due to torsion and distortion. Suetake and Hirashima [10] used extended trigonometric series and an analytical method for box beams with middle diaphragms under various end constraints and loads. Kim and Kim [11] proposed a method to find warping and distortion in TWB with square cross-sections for investigating their statics and free vibration; this theory was extended to multi-cell TWB in [12]. Jang et al. [13] used five field variables (cross-section distortion and warping included) to describe the strain in straight beams and angled joints.

Parallel studies on TWB with RHS were performed by finite element formulations, and the results were compared with those of commercial codes. Carrera et al. [14,15] used the so-called Carrera Unified Formulation (CUF) for statics and dynamics of deformable box TWB. Ren et al. [16,17] investigated the distortion caused by localised eccentric loads on simply supported and cantilever box girders with inner diaphragms, accounting for their in-plane shearing.

In the majority of the papers on lateral-torsional buckling (LTB) of TWB with RHS, the cross-sections are considered rigid in their own plane (e.g., Vo and Lee [18-20], N.-I. Kim et al. [21], Piovan and Machado [22], Lanc et al. [23]). Camotim et al. [24-30] relaxed such assumption, assessing local and global buckling of prismatic TWB by the generalised beam theory (GBT). To the same aim, Kim et al. [31] effectively adopted the higher-order beam theory (HoBT).

Shen et al. [32-35] investigated mixed buckling of RHS beams analytically, while Yang et al. [36,37] did it experimentally. Saoula et al. [38] applied Ritz and Galerkin's techniques to the coupled differential equations describing how distortion affects the lateral buckling of box TWB under combined bending and compression. Szymczak and Kujawa [39,40] obtained closed-form analytical solutions for the critical stresses of TWB with both isotropic and composite square hollow section (SHS), with and without internal walls.

The present investigation extends and completes a previous work of ours [41], where we approach the simplest pattern scheme of TWB with RHS, that is, a simply supported element under uniform transverse load. Indeed, in [41] we introduce the model and a resolution technique based on the so-called homotopy perturbation method (HPM). The advantages of HPM over the iterative Newton–Raphson method with arc length, widely used in FEM commercial codes, is related to its effectiveness to get a rapid and correct non-linear solution, regardless of the degree of non-linearity of the

considered problem; more details about the HPM will be presented later in section 2.1.2. Then, we test the validity of these theoretical and numerical approaches in the above quoted basic structural problem, accompanied by some comparisons with results of the literature. On the other hand, in this paper we first wish to enlarge the class of investigated problems, in that we consider the same structural element under different loads, among which possibly eccentric concentrated forces and couples at the beam ends, in addition to possibly eccentric distributed loads (in both cases, eccentricity is with respect to the centroid-shear centre): this conforms to a larger set of structural problems of interest in design and applications. Consequently, the aim of this paper is twofold: on the one hand, we get closed-form expressions for the transverse mixed buckling (i.e., LTB) of steel TWB with RHS exhibiting distortion. On the other hand, a different and more computationally efficient technique is adopted here, always based on the HPM, which is able to both predict the critical point and describe the post-buckling non-linear path of the considered element, taking into account the cross-section deformation. Eventually, the accuracy of this method and the effect of distortion on the critical value of the applied end moment is discussed and commented, especially with reference to the already existing norms on steel constructions, with an aim towards technical design and applications.

2. A simply supported TWB with deformable RHS

A straight steel TWB with length L and RHS of width b, height h and uniform wall thickness t, Fig. 1(A), is simply supported. The beam is perfect from both material and geometrical viewpoints, and is referred to two orthogonal coordinate frames: (x,y,z)-global, (x,s,n)-local. The position r_n of a point M of the midline of the RHS is at an angle β with the z-axis, Fig. 1 (B). The abscissa s runs anti-clockwise along the midline; n is orthogonal to s. The global coordinate system originates at the centroid of one of the beam ends; since the RHS is twice symmetric, this point coincides with the shear centre.

(A)   (B)
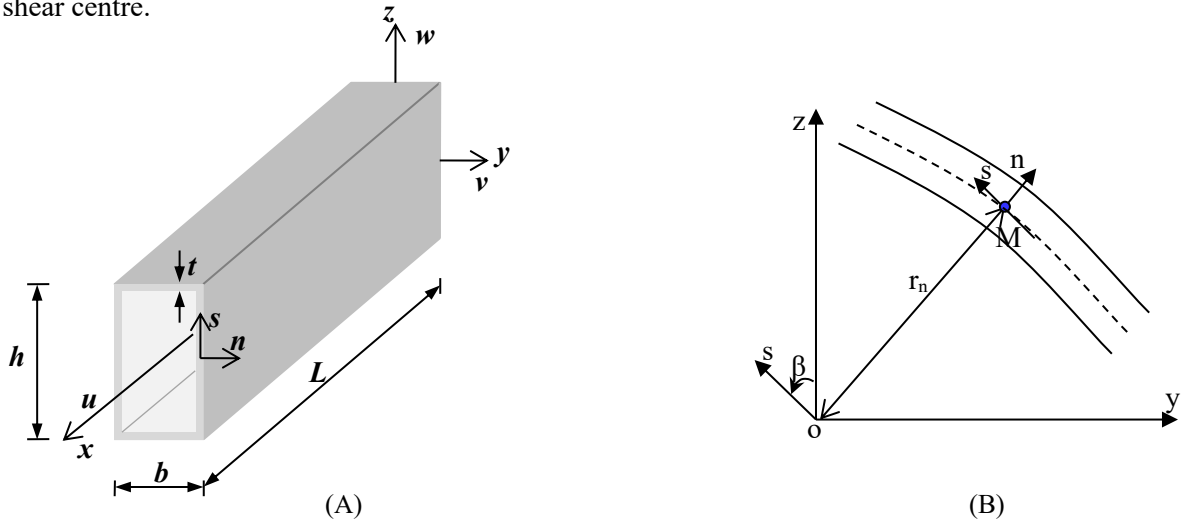
Fig. 1: Geometry of a TWB with RHS and relevant coordinate frames.

Basing on recent literature on refined models for TWB, e.g., Rui et al. [24], Saoula et al. [38] and Librescu and Song [42], we assume that: a) cross-sections may deform; b) shearing in flexure is negligible; c) the angle of twist is finite, while the displacement in distortion are small; d) twist and distortion are coupled. Then, by the assumptions a) and b) the displacement components u_x, u_s, u_n of any point M along x, s, n, respectively, are given by

$$u_x = u - y(v'\cos\theta + w'\sin\theta) + z(v'\sin\theta - w'\cos\theta) - \psi_w\theta' \tag{1a}$$

$$u_s = -v\sin\beta + w\cos\beta + r_n\sin\theta - s(1-\cos\theta) + (\psi_{sd} - n\frac{d\psi_{nd}}{ds})\chi \tag{1b}$$

$$u_n = v\cos\beta + w\sin\beta - s\sin\theta - r_n(1-\cos\theta) + \psi_{nd}\chi \tag{1c}$$

where u, v, w are the displacement components of the centroid along x, y, z, respectively; θ, χ are the angles of torsion and distortion respectively, Fig. 2; and primes stand for x-derivatives. The warping function ψ_w in Eq. (1) follows Sokolnikoff [43] and gave accurate results for box beams in [5]

$$\psi_w = -yz + \frac{8h^2}{\pi^3} \sum_{j=0}^{\infty} \frac{\sin(\frac{(2j+1)\pi z}{h})\sinh(\frac{(2j+1)\pi y}{h})\sin(\frac{(2j+1)\pi}{2})}{(2j+1)^3 \cosh(\frac{(2j+1)\pi b}{2h})} \tag{2a}$$
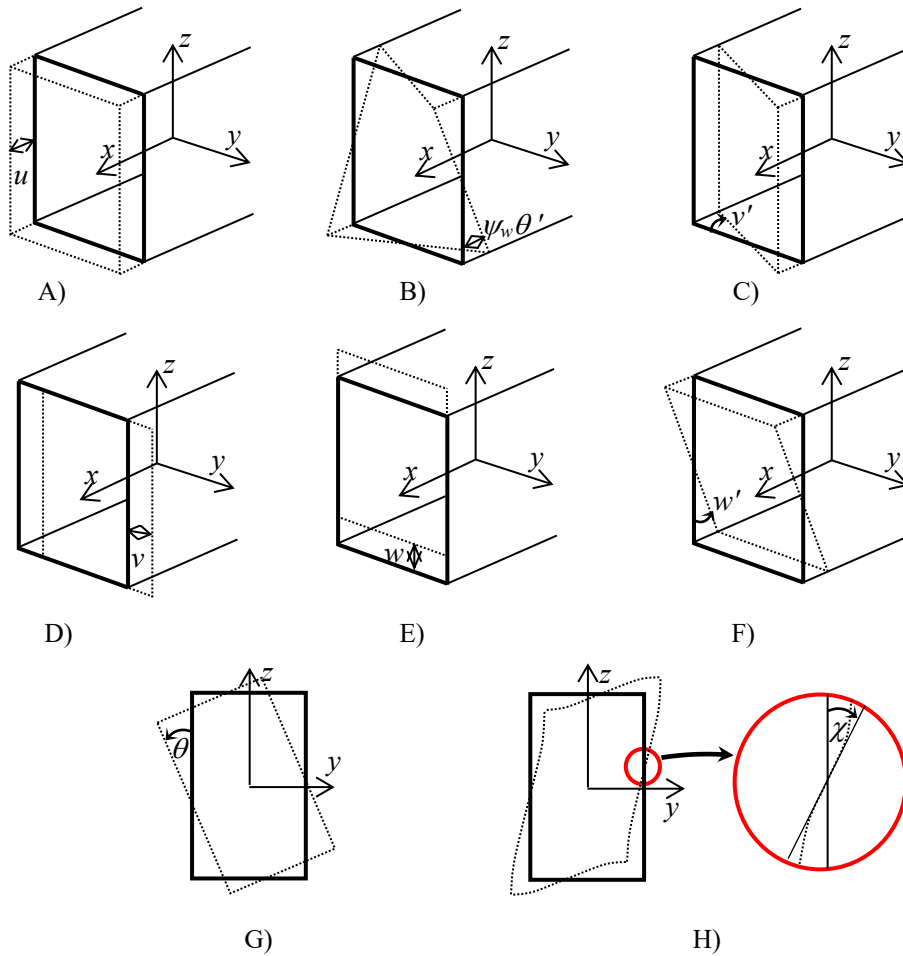
Moreover, the cross-section distortion is the sum of tangential and normal displacement components of the walls, given by ψ_{sd}, ψ_{nd} respectively as in [12,13]

$$\psi_{nd} = \begin{cases} \dfrac{4s^3}{(b+h)b} - \dfrac{(2b+h)s}{b+h} & \text{for the flanges} \\[3mm] -\dfrac{4s^3}{(b+h)h} + \dfrac{(2h+b)s}{b+h} & \text{for the webs} \end{cases} \tag{2b}$$

$$\psi_{sd} = \frac{bh}{b+h}(-1)^{\sin\beta} \tag{2c}$$

and, to end with, the position vector r_n is

$$r_n = z\sin\beta + y\cos\beta \tag{2d}$$

Fig. 2. Cross-section shapes after: A) axial stretch; B) out-of-plane warping; C) bending rotation about z; D) y-deflection; E) z-deflection; F) bending rotation about y; G) torsion rotation; H) in-plane distortion.

Eq. (1) extends the kinematics of Saoula et al. [38] since it considers the finite contributions $\cos(\theta)$, $\sin(\theta)$ instead of their linear counterparts 1, θ, and the relevant non-linear terms. Note that this kinematics has already shown its accuracy in our previous work [41] devoted to the instability of RHS beam under uniform transverse load. Then, a suitable deformation measure is the finite, non-infinitesimal, Green's strain tensor

$$\varepsilon_{kl} = \frac{1}{2}(\frac{\partial u_k}{\partial x_l} + \frac{\partial u_l}{\partial x_k} + \frac{\partial u_m}{\partial x_k}\frac{\partial u_m}{\partial x_l}) \tag{3}$$

Inserting Eq. (1) into Eq. (3), the assumptions c), d) above yield the only non-zero strain components

$$\varepsilon_{xx} = u' - y(v''\cos\theta + w''\sin\theta) - z(w''\cos\theta - v''\sin\theta) - \psi_w\theta'' + \frac{1}{2}(v'^2 + w'^2 + (s^2 + r_n^2)\theta'^2) \tag{4a}$$

$$\gamma_{xs} = (r_n + \frac{d\psi_w}{ds})\theta' + (\psi_{sd} - n\frac{d\psi_{nd}}{ds})\chi' \tag{4b}$$

If the material constituting the beam is homogeneous, isotropic, linearly elastic, Hooke's law provides the normal and tangential stress components σ_{xx}, τ_{xs} in the local coordinates (x,s,n)

$$\sigma_{xx} = E\varepsilon_{xx}, \qquad \tau_{xs} = G\gamma_{xs} \tag{5}$$

where E, G are Young's and shear moduli, respectively.

2.1.   Expended work and balance equations

With the aim of providing a very general investigation on the matter, we consider a wide range of conservative loads on the beam, see Fig. 3: uniformly distributed (UDL); concentrated force (CL) and bending couples $M_y(A)$, $M_y(B)$ (CM). The variation of the external work is thus

$$\delta W = 2\int_0^{\frac{L}{2}} q_z\delta w - q_z e_z\theta\delta\theta + M_x\delta\theta dx + M_y(A)\delta w'(0) + \frac{P}{2}\delta w(\frac{L}{2}) - \frac{P}{2}e_z\theta(\frac{L}{2})\delta\theta(\frac{L}{2}) \tag{6}$$

where e_z is the eccentricity of P and q_z with respect to the shear centre and M_x is a distributed torsion couple that represents an initial imperfection that will be useful for the post-buckling analysis. If A denotes the cross-section area, the variation of the strain energy is

$$\delta U = 2\int_0^{\frac{L}{2}}\iint_A \sigma_{xx}\delta\varepsilon_{xx} + \tau_{xs}\delta\gamma_{xs}dAdx \tag{7}$$
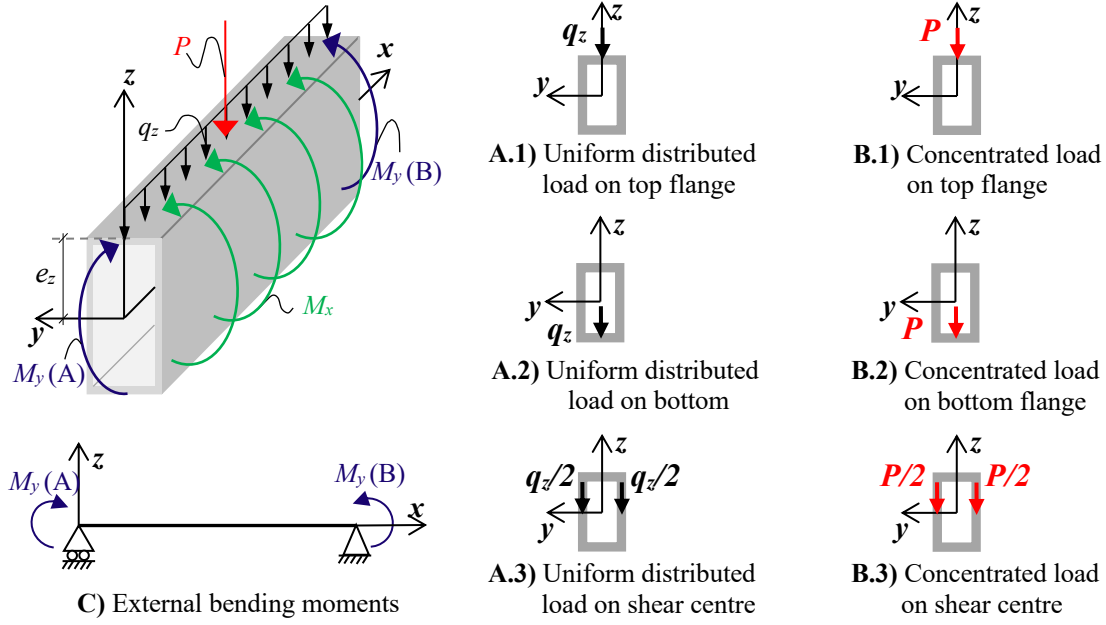
Fig. 3: TWB with RHS under: A) uniform load q_z; B) concentrated load P with eccentricity e_z; C) end bending couples.

Balance is obtained by imposing the stationarity of the total potential energy $\delta(U\text{-}W) = 0$ and using the series expansion of $\cos\theta \approx 1 - \theta^2/2$, $\sin\theta \approx \theta$. Usual procedures lead to

$$\int_0^{\frac{L}{2}} (EI_z v'''' + (EI_z - EI_y)(w''''\theta - v''''\theta^2 + (2w''' - 4v'''\theta)\theta' + (w'' - 2v''\theta)\theta'' - 2v''\theta'^2))\delta v$$

$$+ (EI_y w'''' + (EI_z - EI_y)(v''''\theta + w''''\theta^2 + (2v''' + 4w'''\theta)\theta' + (v'' + 2w''\theta)\theta'' + 2w''\theta'^2) - \alpha_{UDL}q_z)\delta w$$

$$+ (EI_w \theta'''' - G(J - \frac{J_{td}^2}{J_d})\theta'' - \frac{3EI_t}{2}\theta'^2\,\theta'' + (EI_z - EI_y)(w''v'' + (w''^2 - v''^2)\theta) + \alpha_{UDL}q_z e_z\theta - M_x)\delta\theta\, dx$$

$$+ \left[EI_z v''\delta v' - EI_z v'''\delta v + EI_y w''\delta w' - EI_y w'''\delta w + (G(J - \frac{J_{td}^2}{J_d})\theta' - EI_w \theta''')\delta\theta + EI_w \theta''\delta\theta' \right]_0^{\frac{L}{2}}$$

$$+ \alpha_{CM} M_y(A)\delta w'(0) + \alpha_{CL}(-\frac{P}{2}\delta w(\frac{L}{2}) + \frac{P}{2}e_z\theta(\frac{L}{2})\delta\theta(\frac{L}{2})) = 0 \qquad (8)$$

The tracers (α_{UDL}, α_{CL}, α_{CM}) take the values (1,0,0), (0,1,0), (0,0,1) according to the loading case UDL, CL, CM, respectively. The quantities I_y, I_z, I_w, J, I_t, J_d, J_{td} are the moments of inertia with respect to the y and z axes, the warping constant, the Saint-Venant torsion constant, the higher order torsion constant, the distortion and the coupled torsion-distortion constants, given by

$$I_y = \iint_A z^2 dA \qquad (9a)$$

$$I_z = \iint_A y^2 dA \qquad (9b)$$

$$I_w = \iint_A \psi_w^2 dA \qquad (9c)$$

$$J = \iint_A (r_n - \frac{d\psi_w}{ds})^2 dA \qquad (9d)$$

$$I_t = \iint_A (s^2 + r_n^2)^2 \, dA - \frac{(I_y + I_z)^2}{A} \tag{9e}$$

$$J_d = \iint_A (\psi_{sd} - n\frac{d\psi_{nd}}{ds})^2 \, dA \tag{9f}$$

$$J_{td} = \iint_A (\psi_{sd} - n\frac{d\psi_{nd}}{ds})(r_n - \frac{d\psi_w}{ds}) \, dA \tag{9g}$$

Consequently, the equilibrium equations are easily derived:

$$EI_z v'''' + (EI_z - EI_y)(w''''\theta - v''''\theta^2 + (2w''' - 4v'''\theta)\theta' + (w'' - 2v''\theta)\theta'' - 2v''\theta'^2) = 0 \tag{10a}$$

$$EI_y w'''' + (EI_z - EI_y)(v''''\theta + w''''\theta^2 + (2v''' + 4w'''\theta)\theta' + (v'' + 2w''\theta)\theta'' + 2w''\theta'^2) - \alpha_{UDL}q_z = 0 \tag{10b}$$

$$EI_w \theta'''' - G(J - \frac{J_{td}^2}{J_d})\theta'' - \frac{3EI_t}{2}\theta'^2\theta'' + (EI_z - EI_y)(w''v'' + (w''^2 - v''^2)\theta) + \alpha_{UDL}q_z e_z \theta - M_x = 0 \tag{10c}$$

Moreover, the following sets of boundary conditions are obtained:

At x=0

$$\delta v = 0 \quad or \quad v''' = 0$$
$$\delta v' = 0 \quad or \quad v'' = 0$$
$$\delta w = 0 \quad or \quad w''' = 0$$
$$\delta w' = 0 \quad or \quad EI_y w'' + \alpha_{CM}M_y(A) = 0 \tag{11a}$$
$$\delta\theta = 0 \quad or \quad G(J - \frac{J_{td}^2}{J_d})\theta' - EI_w\theta''' = 0$$
$$\delta\theta' = 0 \quad or \quad \theta'' = 0$$

At x=L/2

$$\delta v = 0 \quad or \quad v''' = 0$$
$$\delta v' = 0 \quad or \quad v'' = 0$$
$$\delta w = 0 \quad or \quad EI_y w''' + \alpha_{CL}\frac{P}{2} = 0 \tag{11b}$$
$$\delta w' = 0 \quad or \quad w'' = 0$$
$$\delta\theta = 0 \quad or \quad G(J - \frac{J_{td}^2}{J_d})\theta' - EI_w\theta''' + \frac{P}{2}e_z\theta = 0$$
$$\delta\theta' = 0 \quad or \quad \theta'' = 0$$

2.1.1. Mixed (lateral-torsional) buckling

The non-linear problem in Eq. (10) is tackled by Galerkin's method; the comparison functions for simply supported beams are known to be, once v_0, w_0, θ_0 are unknown amplitudes,

$$\{v, w, \theta\} = \left\{v_0 \sin(\frac{\pi x}{L}), w_0 \sin(\frac{\pi x}{L}), \theta_0 \sin(\frac{\pi x}{L})\right\} \tag{12}$$

Inserting Eq. (12) into Eq. (10) and performing the integration provides the tangent stiffness matrix (also called the Jacobian matrix) $[K(M_0, e_z)]$ at the fundamental state $\{v_0, w_0, \theta_0\} = \{0, w_0, 0\}$

$$K = \begin{bmatrix} \dfrac{\pi^2 EI_z}{L^2} & 0 & \dfrac{8\pi E w_0 (I_z - I_y)}{3L^2} \\[2ex] 0 & \dfrac{\pi^2 EI_y}{L^2} & 0 \\[2ex] \dfrac{8\pi E w_0 (I_z - I_y)}{3L^2} & 0 & \dfrac{3E\pi^2 w_0^2 (I_z - I_y)}{4L^2} + \dfrac{EI_w \pi^2 + GJL^2}{L^2} - \dfrac{GJ_{td}^2}{J_d} + F \end{bmatrix} \quad (13)$$

with the positions

$$F = (\alpha_{UDL} + \alpha_{CL})\frac{8M_0 e_z}{\pi^2} + \alpha_{CM}, \qquad w_0 = \alpha_{UDL}\frac{5M_0 L^2}{48EI_y} + \alpha_{CL}\frac{M_0 L^2}{12EI_y} + \alpha_{CM}\frac{M_0 L^2}{8EI_y}, \quad (14)$$

where M_0 is the maximum bending moment of the beam. We remark that, since the tangent stiffness is not diagonal, the possible buckling modes are coupled: in general, it is not possible to attain transverse buckling only in bending but in mixed bending and torsion. Moreover, the assumption c) above assures that the only attainable buckling is of global nature.

It is known that the singularity condition for the tangent stiffness, i.e., $\det([K(M_0, e_z)]) = 0$, provides the critical values of the applied load inducing buckling. Imposing such condition and performing some simplifications, we obtain the buckling load in terms of the maximum bending moment

$$M_{cr} = \frac{c_1 \pi^2 EI_z}{L^2}\left[c_2 e_z \pm \sqrt{(c_2 e_z)^2 + \frac{I_w}{I_z} + \frac{L^2 G\left(J - \dfrac{J_{td}^2}{J_d}\right)}{\pi^2 EI_z}} \right] \quad (15)$$

If the cross-section has major inertia about y, which is the case considered here, that goes in favour of lateral buckling, and c_1 and c_2 in Eq. (15) reduce to the values provided by Eurocode 3 [44].

$$c_1 = \begin{cases} \dfrac{3\pi^4}{256} \cong 1.14 \; UDL \\[2ex] \dfrac{3619}{27\pi^4} \cong 1.37 \; CL \\[2ex] \dfrac{3}{\pi} \cong 0.95 \; CM \end{cases} \quad (16a)$$

$$c_2 = \begin{cases} \dfrac{3\pi^2}{64} \cong 0.46 \; UDL \\[2ex] \dfrac{18}{\pi^3} \cong 0.58 \; CL \\[2ex] 0 \qquad CM \end{cases}$$

(16b)

Remark that the analogous expressions for the critical value of the maximum bending moment that we find in the literature on the stability of metallic TWB (Eurocode 3 [44], Mohri et al. [45], plus others) can be obtained from the closed-form Eq. (15) by neglecting the distortion ratio J_{td}^2/J_d. It is then very important to remark that: i) the expression in Eq. (15) is original; and ii) its accounting for the distortion ratio with an intrinsic "minus" sign reveals that the distortion has a softening effect on the considered structure, since it lowers the critical value of M_0: this has a mechanical interpretation and a physical justification, since additional possible deformations imply a softer structural element.

2.1.2. Homotopic investigation of equilibrium paths

A thorough investigation of elastic static instability should include post-critical equilibrium paths, which are often neglected since the governing equations for the post-critical region are non-linear and coupled, thus posing analytical difficulties. One means of providing approximate and hierarchic solutions to such non-linear problems is the so-called homotopic perturbation method (HPM), see, e.g., He [46]. This method is based on a series expansion of the (generally finite, non-linear) governing equations of the considered mechanical problem in terms of a (generally) non-physical scalar parameter p. In this way, one obtains a hierarchy of linear equations at different p-orders, to be solved in succession with much easier calculations with respect to the starting set. The HPM differs from other perturbation techniques (for instance, those used in [47] for investigating buckling and post-buckling of elastic beams and frames) in that: a) there is no need for the parameter p to be an actual (small) physical parameter (a strain measure, for instance); b) there is an actual possibility to check the convergence of the series expansion; c) it holds for both weak and strong non-linear problems; d) it has been recently introduced in computer algebra systems for its effectiveness; for details, one may refer to [48,49]. In our case, once posed $p \in \{0,1\}$ the homotopic parameter, the non-linear problem in Eq. (10) is expressed as

$$(1-p)(EI_z v'''') + p[(EI_z - EI_y)(w''''\theta - v''''\theta^2$$
$$+(2w''' - 4v'''\theta)\theta' + (w'' - 2v''\theta)\theta'') - 2v''\theta'^2) + EI_z v''''] = 0 \tag{17a}$$

$$(1-p)(EI_y w'''') + p[(EI_z - EI_y)(v''''\theta + w''''\theta^2$$
$$+(2v''' + 4w'''\theta)\theta' + (v'' + 2w''\theta)\theta'') + 2w''\theta'^2) + EI_y w'''' - \alpha_{UDL} q_z] = 0 \tag{17b}$$

$$(1-p)(EI_w \theta'''' - G(J - \frac{J_{td}^2}{J_d})\theta'') + p[EI_w \theta'''' - G(J - \frac{J_{td}^2}{J_d})\theta'' - \frac{3EI_t}{2}\theta'^2\theta''$$
$$+(EI_z - EI_y)(w''v'' + (w''^2 - v''^2)\theta) - M_x + \alpha_{UDL} q_z e_z \theta] = 0 \tag{17c}$$

The linear path corresponds to $p=0$, the fully non-linear (within the limits of the assumptions introduced) path corresponds to $p=1$; as p ranges from 0 to 1, the whole solution is swept. This technique was already used for other non-linear problems [49-51]. The solutions of Eq. (17) are written as a power series in p

$$v = \sum_{i=0}^{m} p^i v_i, \quad w = \sum_{i=0}^{m} p^i w_i, \quad \theta = \sum_{i=0}^{m} p^i \theta_i \tag{18}$$

and replaced into Eq. (17). Then, collecting the terms of equal powers p^i leads, similarly to what is done in other perturbation methods, to a hierarchy of equations, the first set of which is related to p^0

$$EI_z v_0'''' = 0 \tag{19a}$$
$$EI_y w_0'''' - \alpha_{UDL} q_z = 0 \tag{19b}$$
$$EI_w \theta_0'''' - G(J - \frac{J_{td}^2}{J_d})\theta_0'' - M_x = 0 \tag{19c}$$

the second set is related to p^1

$$EI_z v_1'''' + (EI_z - EI_y)(w_0''''\theta_0 - v_0''''\theta_0^2 + (2w_0''' - 4v_0'''\theta_0)\theta_0' + (w_0'' - 2v_0''\theta_0)\theta_0'') - 2v_0''\theta_0'^2) = 0 \tag{19d}$$

$$EI_z w_1'''' + (EI_z - EI_y)(v_0''''\theta_0 + w_0''''\theta_0^2 + (2v_0''' + 4w_0'''\theta_0)\theta_0' + (v_0'' + 2w_0''\theta_0)\theta_0'') + 2w_0''\theta_0'^2) = 0 \tag{19e}$$

$$EI_w \theta_1'''' - G(J - \frac{J_{td}^2}{J_d})\theta_0'' - \frac{3EI_t}{2}\theta_0'^2\theta_0'' + (EI_z - EI_y)(w_0''v_0'' + (w_0''^2 - v_0''^2)\theta_0) + \alpha_{UDL} q_z e_z \theta_0 = 0 \tag{19f}$$

Eqs. (19) suffice to find the buckling loads of interest in the considered problem and to provide an insight on the post-buckling path, since they describe the fundamental path and its critical points, as well as the first branch of the bifurcated path. Then, the sets related to p^i, $i \geq 2$, are not reported here.

The boundary conditions for simply supported beams are

$$\begin{cases} v_i(0) = 0 \\ v_i''(0) = 0 \\ v_i'(\frac{L}{2}) = 0 \\ v_i'''(\frac{L}{2}) = 0 \end{cases} \tag{20a}$$

$$\begin{cases} w_i(0) = 0 \\ EI_y w_i''(0) + \alpha_{CM} M_y(A) = 0 \\ w_i'(\frac{L}{2}) = 0 \\ EI_y w_i'''(\frac{L}{2}) - \alpha_{CL}\frac{P}{2} = 0 \end{cases} \tag{20b}$$

$$\begin{cases} \theta_i(0) = 0 \\ \theta_i''(0) = 0 \\ \theta_i'(\frac{L}{2}) = 0 \\ G(J - \frac{J_{td}^2}{J_d})\theta_i'(\frac{L}{2}) - EI_w\theta_i'''(\frac{L}{2}) + \alpha_{CL}\frac{P}{2}e_z\theta_i(\frac{L}{2}) = 0 \end{cases} \tag{20c}$$

For solving the hierarchy in Eqs. (19), the linear solutions v_0, w_0, θ_0 are easily obtained by inserting the relevant boundary conditions in Eq. (20) into the homogeneous solutions of Eqs. (19a-c). Once v_0, w_0, θ_0 are replaced into Eqs. (19d-f) we obtain v_1, w_1, θ_1, and so on. To validate the accuracy of the HPM, the non-linear Eqs. (10) are solved by the well-known iterative Newton–Raphson method with arc length. The expressions of the coefficients K_{ij} of the tangent stiffness symmetric matrix are reported in the Appendix.

3. Results and discussion
3.1. LTB moment with distortion

For a validation of the closed-form expression in Eq. (15), we compare the values it provides with those obtained by both GBT and Eurocode 3 [44]. For this comparison we take a beam with E=210 GPa, G=80.77 GPa, h=0.5 m, b=0.15 m, while L and t vary as in Tables 1-7. The GBT results are provided by the GBTUL 2.0 code [52]; the beam is discretized longitudinally into 10 elements and transversally into 4 natural nodes, 3 intermediate nodes for each flange and 5 intermediate nodes for each web. Since short beams undergo local buckling, by assumption c) we do not account for beams with length $L< 8$ m. In Tables 1-7 the comparison is quantitatively measured by the relative errors

$$\Delta 1 = \frac{|(present\ M_{cr}) - GBT|}{Min(present\ M_{cr}, GBT)} \tag{21a}$$

$$\Delta 2 = \frac{|(present\ M_{cr}) - (Eurocode3)|}{Min(present\ M_{cr}, Eurocode3)} \tag{21b}$$

The comparison manifestly shows that the differences between the present results and those of GBT are quite acceptable, in that the relative error $\Delta 1$ varies from 1% to 9%. However, it is rather remarkable that, since Eurocode 3 neglects the effect of the cross-section distortion, its results grossly overestimate the critical moment inducing LTB, since the relative error $\Delta 2$ can reach 20%. It is apparent that the cross-section distortion affects the structural stability of TWB with RHS in a significant manner: thus, neglecting this effect can be crucial for design purposes of beams with deformable cross-sections.

This result is not surprising, however, and fully reflects the physical phenomenon: indeed, admitting that the structural element undergoes several ways of deformation means that it is somehow 'softer' with respect to the same structural element subjected to inner constraints such as that of rigid cross-sections. Then, its elastic stiffnesses are inevitably lower than that of the beam not affected by cross-section distortion, and this affects both the tangent stiffness and the buckling load in the sense that the latter will inevitably be lower – i.e., the onset of instability can be reached much before than expected, which is obviously undesirable from a technical viewpoint.

Table 1: Buckling moments (kNm) for UDL, load applied on top flange, $e_z = 0.25$ m

L (m)	t (cm)	Present Eq. (15)	GBT	Eurocode 3	Δ1	Δ2
8.00	1.50	7264.34	6990.41	8680.87	4%	20%
	2.00	9688.89	10156.12	11574.49	5%	19%
10.00	1.50	5866.16	6028.42	7000.69	3%	19%
	2.00	7824.03	8548.01	9334.25	9%	19%

Table 2: Buckling moments (kNm) for UDL, load applied at the centroid, $e_z = 0.0$ m

L (m)	t (cm)	Present Eq. (15)	GBT	Eurocode 3	Δ1	Δ2
8.00	1.50	7648.25	7330.54	9066.36	4%	19%
	2.00	10200.76	10623.55	12088.48	4%	18%
10.00	1.50	6113.15	6251.64	7248.49	2%	18%
	2.00	8153.35	8854.48	9664.66	8%	18%

Table 3 : Buckling moments (kNm) for UDL, load applied on bottom flange, $e_z = -0.25$ m

L (m)	t (cm)	Present Eq. (15)	GBT	Eurocode 3	Δ1	Δ2
8.00	1.50	8052.44	7683.51	9468.96	5%	18%
	2.00	10739.68	11105.45	12625.29	3%	17%
10.00	1.50	6370.54	6479.68	7505.06	2%	18%
	2.00	8496.54	9167.44	10006.76	7%	18%

Table 4: Buckling moments (kNm) for CL, load applied on top flange, $e_z = 0.25$ m

L (m)	t (cm)	Present Eq. (15)	GBT	Eurocode 3	Δ1	Δ2
8.00	1.50	8613.61	7884.66	10314.80	9%	20%
	2.00	11488.52	11650.52	13753.06	1%	19%
10.00	1.50	6974.30	6915.82	8337.15	1%	19%
	2.00	9302.05	9926.68	11116.20	6%	19%

Table 5: Buckling moments (kNm) for CL, load applied at the centroid, $e_z = 0.0$ m

L (m)	T (cm)	Present Eq. (15)	GBT	Eurocode 3	Δ1	Δ2
8.00	1.50	9191.32	8411.75	10895.53	9%	19%
	2.00	12258.81	12405.53	14527.38	1%	18%
10.00	1.50	7346.51	7292.40	8710.90	1%	18%
	2.00	9798.32	10438.79	11614.54	6%	18%

Table 6 : Buckling moments (kNm) for CL, load applied on bottom flange, $e_z = -0.25$ m

L (m)	T (cm)	Present Eq. (15)	GBT	Eurocode 3	Δ1	Δ2
8.00	1.50	9807.77	9261.85	11508.96	5%	17%
	2.00	13080.74	13401.02	15345.28	2%	17%
10.00	1.50	7738.57	7779.49	9101.41	1%	18%
	2.00	10321.07	11031.36	12135.22	7%	17%

Table 7: Buckling moments (kNm) for CM

L (m)	T (cm)	Present Eq. (15)	GBT	Eurocode 3	Δ1	Δ2
8.00	1.50	6373.54	5842.97	7555.29	9%	19%
	2.00	8500.63	9303.75	10073.73	9%	19%
10.00	1.50	5094.29	5453.04	6040.41	7%	19%
	2.00	6794.46	7398.68	8053.88	9%	19%

3.2. Pre- and post-buckling analysis and comparison

We now compare the equilibrium paths provided by the HPM, Newton-Raphson and FEM for a beam with L=10 m, b=0.15 m, h=0.5 m, t=0.015 m, commenting also the effect of distortion on non-linear equilibria. In all computations, the value of M_x, representing the initial imperfection, is assumed to be 10^{-3} kNm. As above, we consider the three loading cases UDL, CL (where the load can be applied to the top flange, bottom flange or at the shear centre), CM.

The non-linear Eqs. (10) is solved by the HPM first, accounting for 80 terms in the power series expansion (i=80). Then, Newton-Raphson method with arc-length which can be uniform and unitary, or reduced if convergence fails, is adopted; the maximum tolerance is 10^{-6}. The FEM simulation is carried out by the commercial code Abaqus [53] with two elements: the first (shell, S8R) is for beams affected by cross-section distortion, while the second (beam, B32H) meshes beams with rigid cross-sections.

Figs. 4–18 show that in TWB with RHS affected by distortion the HPM provides linear non-trivial fundamental paths and bifurcation points that are quite close to those obtained by Newton-Raphson method and FEM (shell element S8R); the maximum relative error is 3%. This error remains acceptable for all non-linear paths (q_z, $w(L/2)$), (q_z, $v(L/2)$), (q_z, $\theta(L/2)$), (P, $w(L/2)$), (P, $v(L/2)$), (P, $\theta(L/2)$)) when the load is applied on the top flange. We also remark only small discrepancies among the results of the three techniques of solving the problem for the post-buckling equilibrium paths (q_z, v_0), (q_z, $\theta(L/2)$), (P, $v(L/2)$) and (P, $\theta(L/2)$), (q_z, $v(L/2)$), (q_z, $\theta(L/2)$) of the beams loaded at the bottom flange and at the centroid-shear centre; the same happens for the equilibria (M_y(A), $v(L/2)$), (M_y(A), $\theta(L/2)$)). In the non-linear equilibria (q_z, $w(L/2)$), (P, $w(L/2)$), (M_y(A), $w(L/2)$) the difference between the results given by the three methods of solution always increases away from the critical point. It is also worth remarking that the FEM analysis adopting a mesh of shell elements provides only short

post-buckling paths, due to the fact that local buckling occurs near the global bifurcation point; a similar behaviour with analogous comments is in [54] for TWB with open cross-sections.

Figs. 13–18 show that for concentrated loads and end moments the bifurcation points provided by FEM analysis adopting a mesh of beam element are slightly lower than those given by HPM and Newton-Raphson integration, the maximum relative error being about 6%. Once again, we see that neglecting cross-sections distortion overestimates the buckling load with respect to beam kinematics accounting for cross-sections deformation, even adopting the same resolution technique: indeed, the difference between the predictions of HPM with and without distortion for the CL case can reach 26%.

4.   Final remarks

To highlight the influence of distortion on the lateral-torsional buckling and post-buckling behaviour of simply supported steel TWB with RHS under several load conditions, we introduced beam kinematics considering non-infinitesimal displacements, finite twist angles and small distortion angles. The non-linear field equations have been obtained by stationarity conditions on a total potential energy function accounting for linear elastic homogeneous and isotropic behaviour. We have found a new closed-form expression for the critical values of a characteristic moment, extending previous ones from both theoretical and technical literature, including Eurocode 3. In addition, we have compared three methods (HPM, Newton Raphson and FEM) to solve the non-linear field equations and obtain pre- and post-buckling equilibrium paths. The main results are:

1) The differences between the buckling loads obtained by our Eq. (15) and those obtained by the GBT are quite acceptable.
2) The fundamental (linear) paths and the bifurcation points computed by HPM coincide exactly with those provided by Newton-Raphson integration and FEM.
3) Apart from just three post-buckling paths (denoted $(q_z, w(L/2))$, $(P, w(L/2))$ and $(M_0, w(L/2))$ here), which exhibit remarkable differences when evaluated by the three above quoted resolution techniques, the other post-buckling equilibria are quite similar.
4) The present kinematics, accounting for cross-sections distortion, underestimates the buckling load with respect to that of the beam models with rigid cross-sections: thus, our model is conservative.
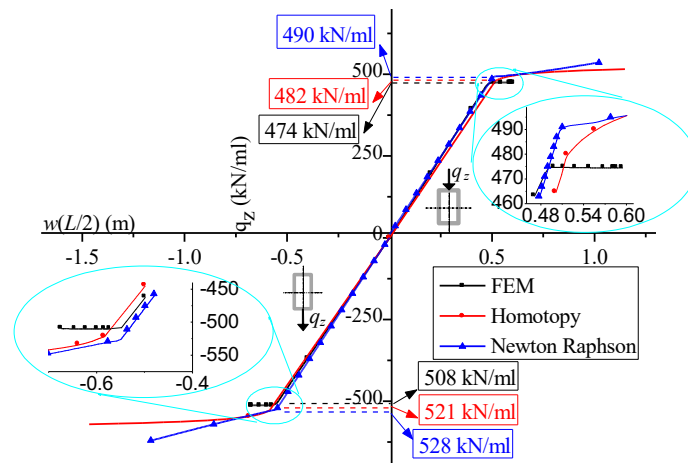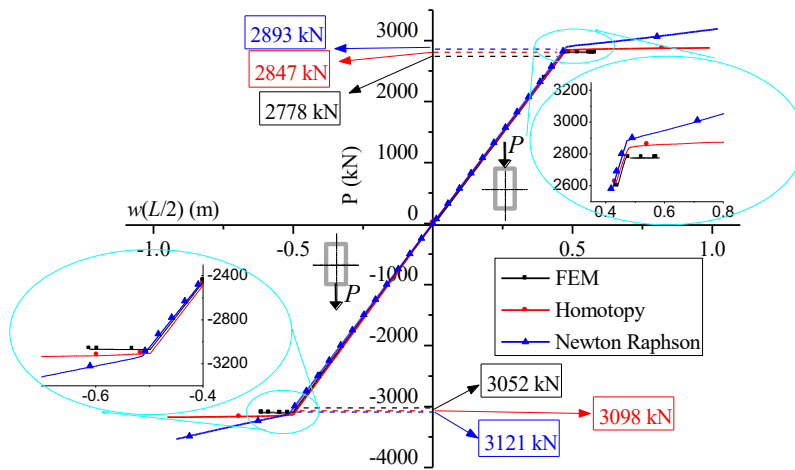

Fig. 4: Pre- and post-buckling equilibrium paths $(q_z, w(L/2))$ with distortion: UDL on top flange (top-right curve), UDL on bottom flange (bottom-left curve).
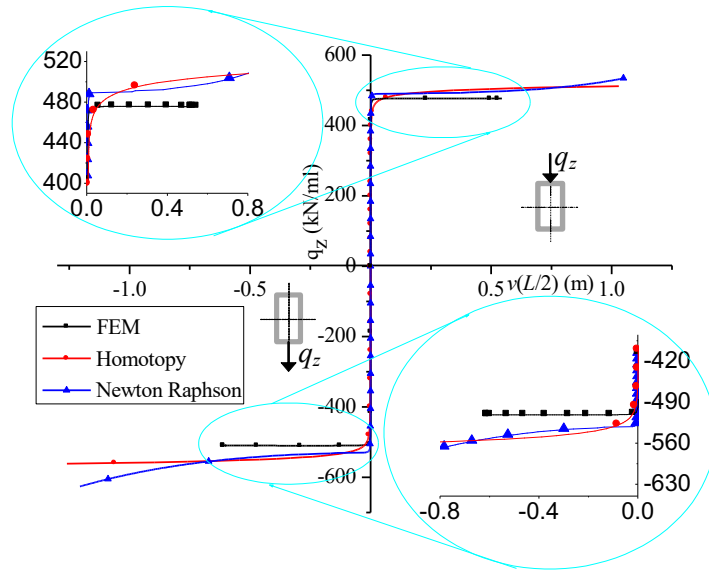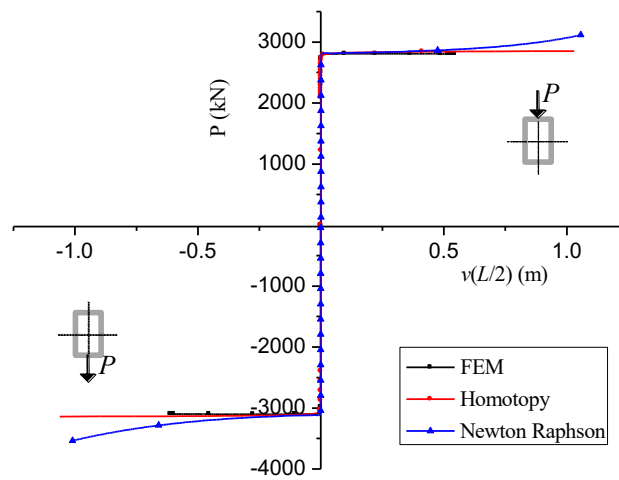
Fig. 5: Pre- and post-buckling equilibrium paths (q_z, $v(L/2)$) with distortion: UDL on top flange (top-right curve), UDL on bottom flange (bottom-left curve).
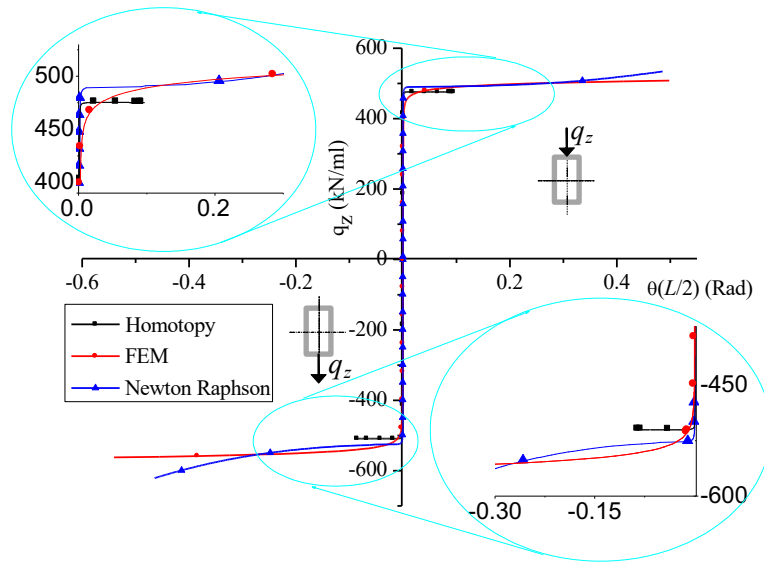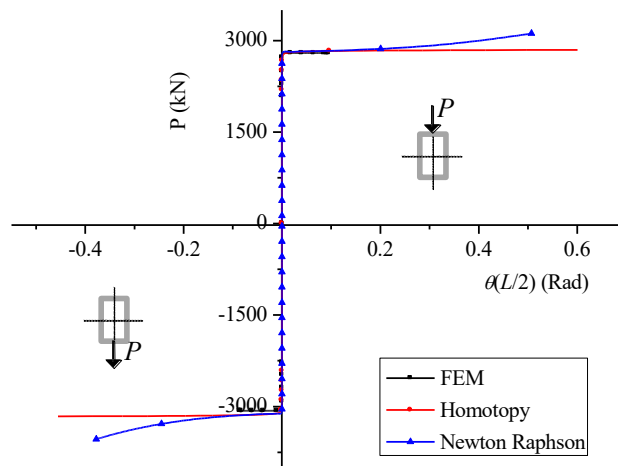

Fig. 6: Pre- and post-buckling equilibrium paths (q_z, $\theta(L/2)$) with distortion: UDL on top flange (top-right curve), UDL on bottom flange (bottom-left curve).
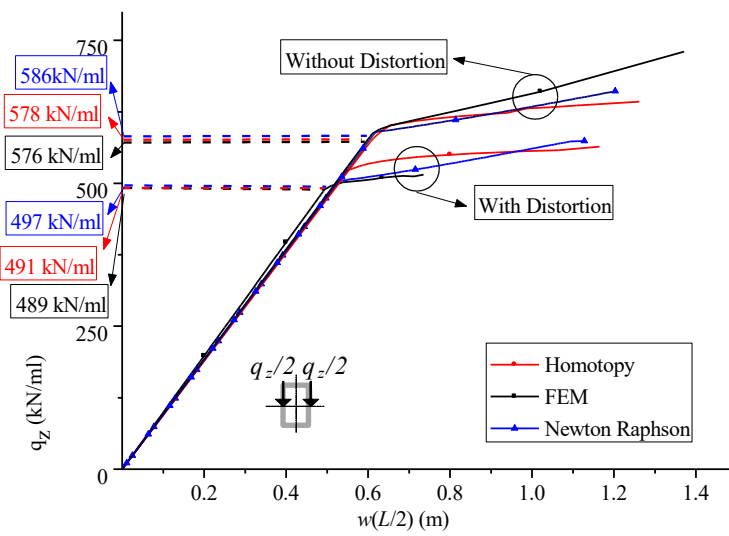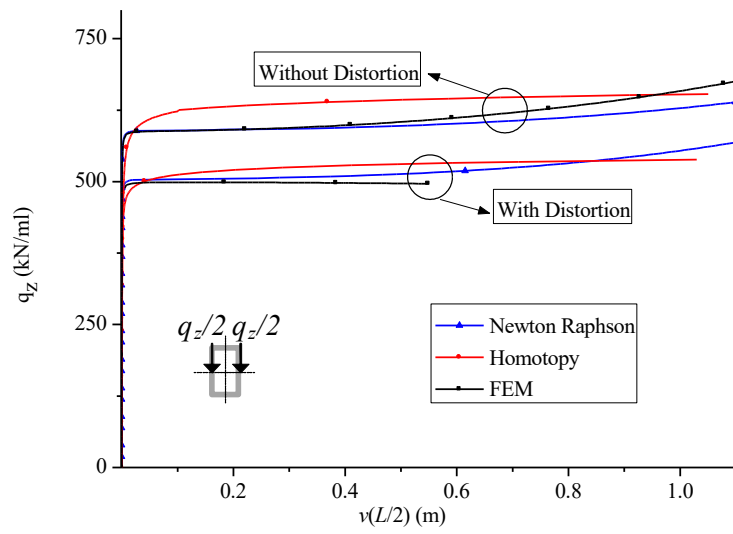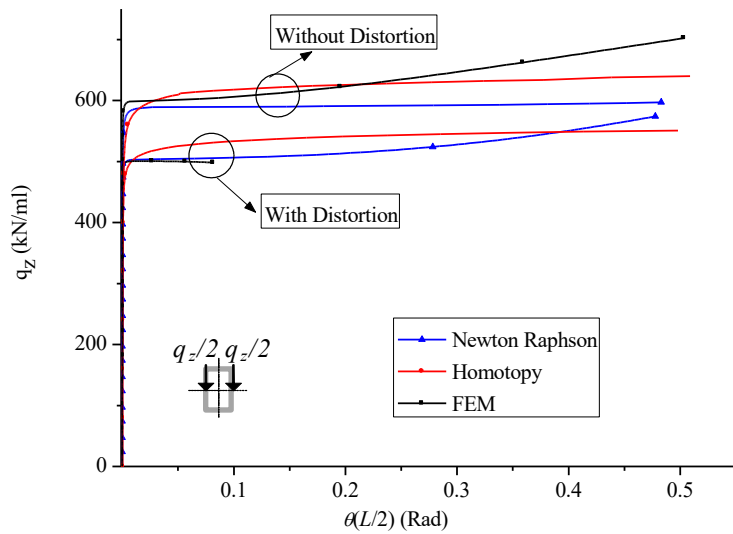
Fig. 7: Pre- and post-buckling equilibrium paths (P, $w(L/2)$) with distortion: CL on top flange (top-right curve), CL on bottom flange (bottom-left curv

Fig. 8: Pre- and post-buckling equilibrium paths (P, $v(L/2)$) with distortion: CL on top flange (top-right curve), CL on bottom flange (bottom-left curve).

Fig. 9: Pre- and post-buckling equilibrium paths (P, $\theta(L/2)$) with distortion: CL on top flange (top-right curve), CL on bottom flange (bottom-left curve).

Fig. 10: Pre- and post-buckling equilibrium paths (q_z, $w(L/2)$) with and without distortion for UDL at the shear centre.
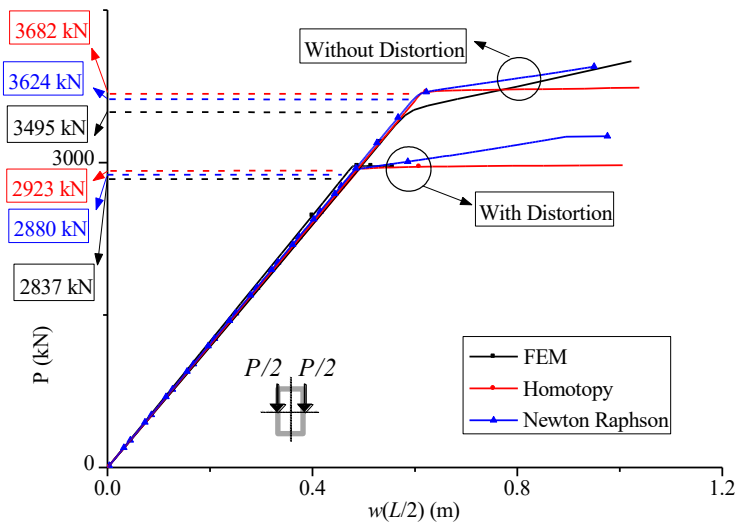
Fig. 11: Pre- and post-buckling equilibrium paths ($q_z, v(L/2)$) with and without distortion for UDL at the shear centre
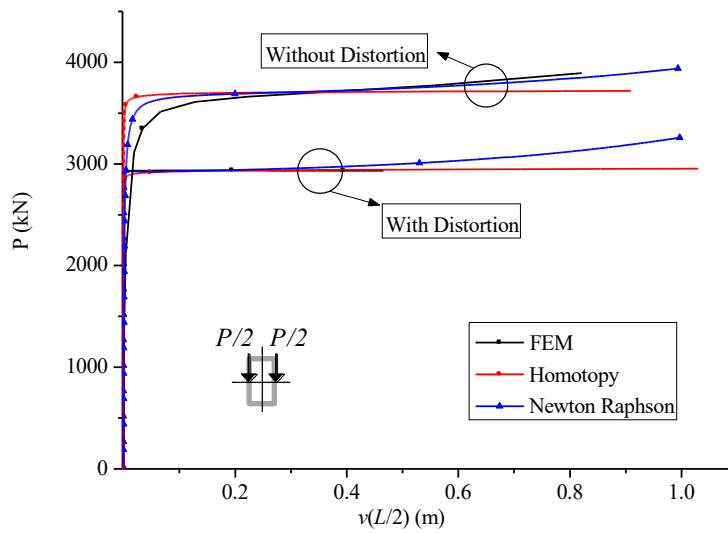

Fig. 12: Pre- and post-buckling equilibrium paths ($q_z, \theta(L/2)$) with and without distortion for UDL at the shear centre.
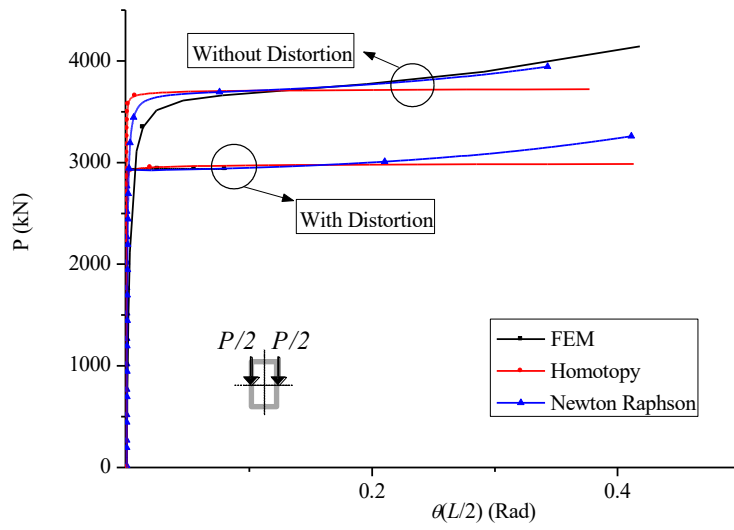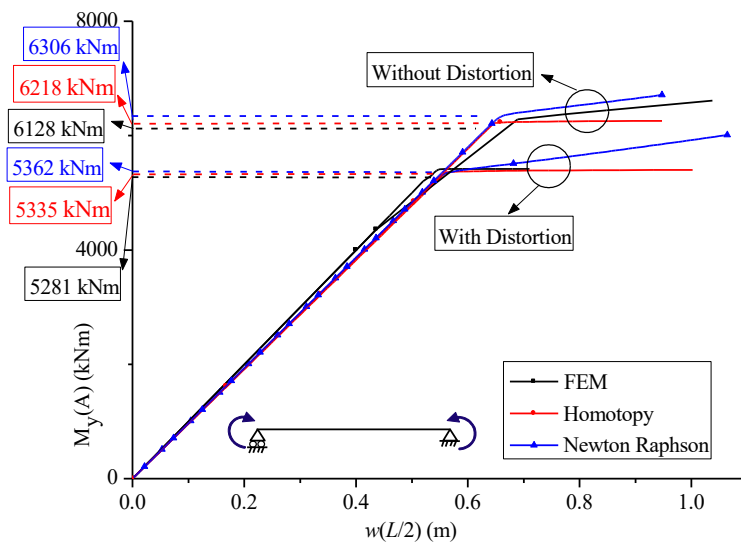
Fig. 13: Pre- and post-buckling equilibrium paths ($P,w(L/2)$) with and without distortion for CL at the shear centre.
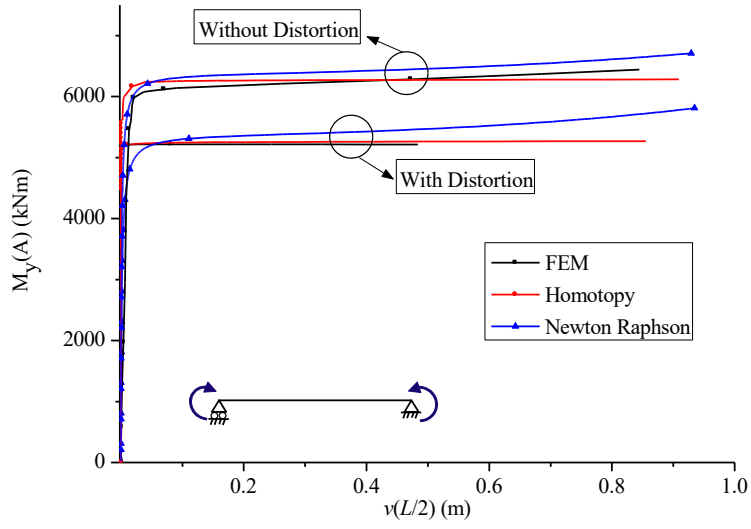

Fig. 14: Pre- and post-buckling equilibrium paths ($P,v(L/2)$) with and without distortion for CL at the shear centre
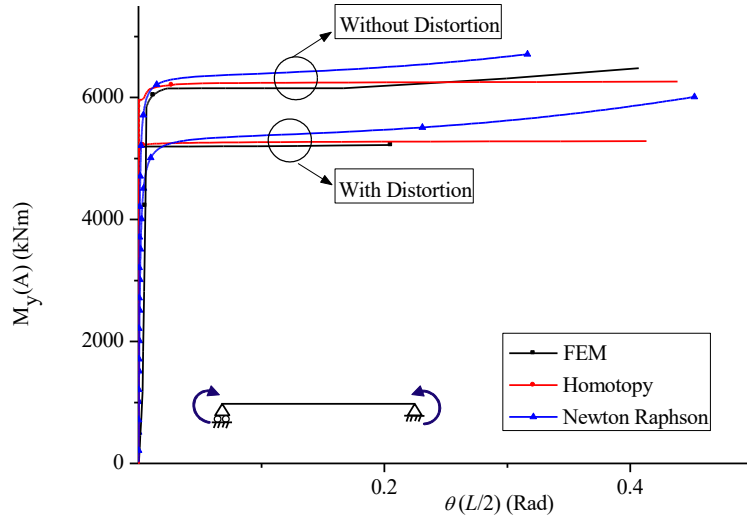
Fig. 15: Pre- and post-buckling equilibrium paths $(P, \theta(L/2))$ with and without distortion for CL at the shear centre.

Fig. 16: Pre and post-buckling equilibrium paths $(M_y(A), w(L/2))$ with and without distortion for CM.

Fig. 17: Pre- and post-buckling equilibrium paths (M_y(A), $v(L/2)$) with and without distortion for CM.

Fig. 18: Pre- and post-buckling equilibrium paths (M_y(A), $\theta(L/2)$) with and without distortion for CM.

Appendix

$$K_{11} = \frac{E\pi^2 (4I_z - 3\theta_{00}^2 (I_z - I_y))}{4L^2}$$

$$K_{12} = \frac{8E\pi\theta_{00}(I_z - I_y)}{3L^2}$$

$$K_{13} = \frac{E\pi(16w_{00} - 9v_{00}\theta_{00}\pi)(I_z - I_y)}{6L^2}$$

$$K_{22} = \frac{E\pi^2(4I_y + 3\theta_{00}^2(I_z - I_y))}{4L^2}$$

$$K_{23} = \frac{E\pi(16v_{00} + 9w_{00}\theta_{00}\pi)(I_z - I_y))}{6L^2}$$

$$K_{33} = \frac{3E\pi^2(w_{00}^2 - v_{00}^2)(I_z - I_y)}{4L^2} + \frac{8EI_w\pi^2 + 9EI_t\pi^2\theta_{00}^2 + 8GJL^2}{8L^2} - \frac{GJ_{td}^2}{J_d} + F$$

$$K_{21} = K_{12}$$

$$K_{31} = K_{13}$$

$$K_{32} = K_{23}$$

References

[1] Vlasov, V. Z. Thin walled elastic beams. Russian original book: Stroizdat, Moscow, 1940. French translation: Pieces longues en voiles minces, Paris: Eyrolles; 1962.

[2] Benscoter, S.U. A theory of torsion-bending for multicell beams J. Appl. Mech. 20 (1954) 25-34.

[3] Smith, E.C. and Chopra, I. Formulation and evaluation of an analytical model for composite box-beams. J. Am. Helicopt. Soc. 36 (1991) 23-35.

[4] H. Shakourzadeh, Y.Q. Guo and J.-L. Batoz. A torsion bending element for thin-walled beams with open and closed cross sections. Computers and structures 55 (1995) 1045-1054.

[5] C. Kim and S. R. White. Thick-walled composite beam theory including 3-D elastic effects and torsional warping. lnt. J. Solids Structures. 34 (1997) 4237-4259.

[6] Loughlan, J and Ata, M. The behaviour of open and closed section carbon fibre composite beams subjected to constrained torsion. Composite Structures 38 (1997) 631-647.

[7] Aniko Pluzsik and Làszlo P. Kollàr. Torsion of closed section, orthotropic, thin-walled beams. International Journal of Solids and Structures. 43 (2006) 5307–5336.

[8] Ziane N., Meftah S.A., Belhadj H.A., Tounsi A., Bedia E.A.A. Free vibration analysis of thin and thick-walled FGM box beams. Int J Mech Sci. 66 (2013) 273–82.

[9] L. Mentrasti. Distortion (and Torsion) of Rectangular Thin-Walled Beams. Thin-Walled Struct. 10 (1990) 175-193

[10] Yoshitaka Suetake and Masaharu Hirashima. Extended trigonometric series analysis of box girders with diaphragms. Journal of Engineering Mechanics. 123 (1997) 293-301.

[11] J. H. Kim and Y. Y. Kim. Analysis of Thin-Walled Closed Beams With General Quadrilateral Cross Sections. Journal of Applied Mechanics 66 (1999) 904-912.

[12] J. H. Kim and Y. Y. Kim. Thin-Walled Multicell Beam Analysis for Coupled Torsion, Distortion, and Warping Deformations. Journal of Applied Mechanics. 68 (2001) 260-269.

[13] G.-W. Jang, K.J. Kim and Y.Y. Kim. Higher-order beam analysis of box beams connected at angled joints subject to out-of-plane bending and torsion. Int. J. Num. Methods In Eng. 75 (2008) 1361-1384.

[14] E. Carrera, A. Pagani, F. Zangallo, Thin-walled beams subjected to load factors and non-structural masses, International Journal of Mechanical Sciences. 81 (2014) 109–119.

[15] D.S. Mashat, E. Carrera, A.M. Zenkour, S.A. Al Khateeb, M. Filippi, Free vibration of FGM layered beams by various theories and finite elements, Composites Part B 59 (2014) 269–278.

[16] Y. Rena, W. Cheng, Y. Wang, B. Wang. Analysis of the distortion of cantilever box girder with inner flexible diaphragms using initial parameter method, Thin-Walled Struct. 117 (2017) 140–154.

[17] Y. Rena, W. Cheng, Y. Wang, Q. Chen, B. Wang. Distortional analysis of simply supported box girders with inner diaphragms considering shear deformation of diaphragms using initial parameter method. Engineering Structures 145 (2017) 44–59.

[18] Thuc Phuong Vo and Jaehong Lee. Free vibration of axially loaded thin-walled composite box beams. Composite Structures 90 (2009) 233–241.

[19] Thuc Phuong Vo and Jaehong Lee, Flexural-torsional buckling of thin-walled composite box beams, Thin-Walled Struct. 45 (9), (2007) 790-798.

[20] T.P. Vo and J. Lee, Interaction curves for vibration and buckling of thin-walled composite box beams under axial loads and end moments, Appl. Math. Modelling 34 (2010) 3142–3157.

[21] Nam-Il Kim, Dong Ku Shin, Young-Suk Park. Coupled stability analysis of thin-walled composite beams with closed cross-section. Thin-Walled Structures 48 (2010) 581–596.

[22] M.T. Piovan and S.P. Machado. Thermo elastic dynamic stability of thin-walled beams with graded material properties. Thin-Walled Structures 49 (2011) 437–447.

[23] Domagoj Lanc, Thuc P. Vo, Goran Turkalj, Jaehong Lee. Buckling analysis of thin-walled functionally graded sandwich box beams. Thin-Walled Structures 86 (2015) 148–156.

[24] B. Rui, C. Basaglia, D. Camotim, R. Gonçalves. GBT buckling analysis of generally loaded thin-walled members with arbitrary flat-walled cross-sections, Thin-Walled Struct. 123 (2018) 11–24.

[25] Gonçalves R, Camotim D. (2004), "Buckling analysis of single and multi-cell closed thin-walled metal members using Generalised Beam Theory", Proceedings Of The Fourth International Conference On Coupled Instabilities In Metal Structures, Rome, 27–29/9.

[26] Gonçalves R, Camotim D. (2010). Steel-concrete composite bridge analysis using generalised beam theory. Steel and Composite Structures 10(3), 223-243.

[27] Silvestre, N. and Camotim, D. (2006). Vibration behaviour of axially compressed cold-formed steel members. Steel and Composite Structures 6(3), 221-236.

[28] R. Gonçalves, D. Camotim, Elastic buckling of uniformly compressed thin-walled regular polygonal tubes, Thin-Walled Struct. 71 (2013) 35–45.

[29] R. Gonçalves, D. Camotim, Buckling behaviour of thin-walled regular polygonal tubes subjected to bending or torsion, Thin-Walled Struct.73 (2013) 185–197.

[30] R. Gonçalves, D. Camotim, On the first-order and buckling behaviour of thin-walled regular polygonal tubes, Steel Construction Designand Research. 9(4) (2016) 279–290.

[31] Do-Min Kim, Soomin Choi, Gang-Won Jang and Yoon Young Kim, Buckling analysis of thin-walled box beams under arbitrary loads with general boundary conditions using higher-order beam theory, Journal of Mechanical Science and Technology. 33 (5) (2019) 2289-2305.

[32] J. Shen, M. A. Wadee, A. J. Sadowski, Interactive buckling in long thin-walled rectangular hollow section struts, Int. J. Non-Linear Mech. 89 (2017) 43–58.

[33] J. Shen, M. A. Wadee, Length effects on interactive buckling in thin-walled rectangular hollow section struts, Thin-Walled Struct. 128 (2018) 152-170.

[34] J. Shen, M. A. Wadee, Imperfection sensitivity of thin-walled rectangular hollow section struts susceptible to interactive buckling, Int. J. Non-Linear Mech. 99 (2018) 112–130.

[35] J. Shen, M. A. Wadee, Sensitivity to local imperfections in inelastic thin-walled rectangular hollow section struts, Int. J. Non-Linear Mech. 17 (2019) 43-57.

[36] Lu Yang, Gang Shi, Menghan Zhao, Wenjing Zhou. Research on interactive buckling behavior of welded steel box-section columns. Thin-Walled Structures 115 (2017) 34–47.

[37] K. Ning, L. Yang, H. Yuan, M. Zhao, Flexural buckling behaviour and design of welded stainless steel box-section beam-columns, Journal of Constructional Steel Research. 161 (2019) 47–56.

[38] A. Saoula, S.A. Meftah, F. Mohri, El Mostafa Daya. Lateral buckling of box beam elements under combined axial and bending loads. Journal of Constructional Steel Research 116 (2016) 141–155.

[39] Czesław Szymczak, Marcin Kujawa. Distortional buckling of thin-walled columns of closed quadratic cross-section. Thin-Walled Structures 113 (2017) 111–121.

[40] Czesław Szymczak, Marcin Kujawa. Distortional buckling of composite thin-walled columns of a box-type cross section with diaphragms. Acta Mech. 230 (2019) 3945–3961.

[41] N. Benmohammed, N. Ziane, S.A. Meftah and G. Ruta. Distortional effect on global buckling and post-buckling behaviour of steel box beams. Steel and Composite Structures 35 (2020) 717-727

[42] L. Librescu and O. Song. Thin-Walled Composite Beams Theory and Application. Springer. 2006.

[43] Sokolnikoff, I.S., *Mathematical Theory of Elasticity*, McGraw-Hill, New York, USA. 1946.

[44] Eurocode 3: European Committee for Standardization. EN1993-1-1, Eurocode 3: design of steel structures. Part1-1: General rules and rules for buildings, Brussels; 2005.

[45] F. Mohri, C. Bouzerira, M. Potier-Ferry. Lateral buckling of thin-walled beam-column elements under combined axial and bending loads. Thin-Walled Structures 46 (2008) 290–302.

[46] J.-H. He. Homotopy perturbation method for solving boundary value problems. Physics Letters A 350 (2006) 87-88.

[47] M. Pignataro, N. Rizzi and A. Luongo. Stability, bifurcation and postcritical behaviour of elastic structures. Elsevier, Amsterdam, 1991.

[48] Liao, S.J. (2003). Beyond Perturbation: Introduction to the Homotopy Analysis Method, Boca Raton: Chapman & Hall/CRC Press.

[49] Liao, S.J. (2012). Homotopy Analysis Method in Nonlinear Differential Equations, Berlin & Beijing: Springer & Higher Education Press.

[50] M. Esmaeilpour, D.D. Ganji. Application of He's homotopy perturbation method to boundary layer flow and convection heat transfer over a flat plate. Physics Letters A 372 (2007) 33–38.

[51] Amin Jafarimoghaddam. On the Homotopy Analysis Method (HAM) and Homotopy Perturbation Method (HPM) for a nonlinearly stretching sheet flow of Eyring-Powell fluids. Engineering Science and Technology, an International Journal. 22 (2019) 439-451.

[52] GBTUL, Version 2.0.4.3, The Generalised Beam Theory Research Group, Instituto superior Técnico, Lisbon, Portugal, 2013.

[53] Abaqus Standard User's Manual, Version 6.4. Hibbit, Karlsson and Sorensen Inc., Pawtucket, RI, USA, 2003 (Abaqus).

[54] Aberrahmane Ed-dinari, Hicham Mottaqui, Bouazza Braikat, Mohammad Jamal, Foudil Mohri, Noureddine Damil. Large torsion analysis of thin-walled open sections beams by the Asymptotic Numerical Method. Engineering Structures 81 (2014) 240–255.